


Cite this: *RSC Adv.*, 2017, 7, 43233

Ionic liquid assisted hydrothermal syntheses of Au doped TiO₂ NPs for efficient visible-light photocatalytic hydrogen production from water, electrochemical detection and photochemical detoxification of hexavalent chromium (Cr⁶⁺)

T. N. Ravishankar,^a *^{ab} Mauricio de O. Vaz,^b T. Ramakrishnappa,^c Sergio R. Teixeira^b and J. Dupont^d

Au/TiO₂ NPs have been successfully prepared at 130 °C in one day using an ionic liquid assisted hydrothermal method using methoxyethyl methyl imidazolium methanesulfonate as the ionic liquid, titanium(IV) isopropoxide and tetrachloroaurate(III) trihydrate as precursors. Physico-chemical properties of the obtained photocatalysts were investigated via thorough characterizations. The framework substitution of Au in TiO₂ NPs was established by X-ray diffraction (XRD), X-ray photoelectron spectroscopy (XPS) and energy dispersive X-ray spectroscopy (EDS) techniques. X-ray diffraction (XRD) and transmission electron microscopy (TEM) image results confirmed the anatase phase and nanocrystalline nature of Au/TiO₂. The optical properties revealed an extended tailing of the absorption edge toward the visible region upon Au doping. The concentration of Au in the TiO₂ matrix has been fine-tuned to improve the hydrogen production, electrochemical detection and photochemical detoxification of hexavalent chromium (Cr⁶⁺). But there are no reports utilizing a single material for all three applications such as photocatalytic hydrogen production from water and photochemical as well as electrochemical reduction of Cr⁶⁺ to Cr³⁺. The synergy between the Au and TiO₂ has an optimum for concentration of 0.5 wt% Au doped TiO₂. The optimized product has produced promising hydrogen evolution of 3344 μmol g⁻¹ under illumination with a visible light source in a water/ethanol system. The optimized product has shown promising electrocatalytic reduction and the photocatalytic detoxification ability of the material towards Cr⁶⁺ was explored. Amperometric studies showed a linear range from 0.1 to 2.7 mM, and limits of detection and quantification of 0.01 mM and 0.023 mM, respectively. The Au/TiO₂ nanoparticle modified glassy carbon has been used for electrochemical monitoring of Cr⁶⁺ in natural water samples. The material also showed better photochemical reduction of Cr⁶⁺ in sunlight compared to UV light.

Received 2nd May 2017
Accepted 24th August 2017

DOI: 10.1039/c7ra04944g

rsc.li/rsc-advances

Introduction

The continual increase in world population and lifestyle standards has led to a sharp increase in global energy consumption. The conventionally used fossil fuels are costly and present environmental limitations so the efficient utilization of renewable energy sources is more urgent. In this regard,

photocatalytic water splitting hydrogen production has been considered as having enormous potential for the sustainable development of society. Several semiconducting metal oxide NPs have been utilized for photocatalytic hydrogen production.^{1–3} Amongst these TiO₂ has been widely used as a photocatalyst for hydrogen generation via water splitting because of its wideband gap ($E_g = 3.2$ eV), low-cost, non-toxicity and good oxidizing power.⁴ However, literature reports suggested that TiO₂ has some practical limitations, for example bare TiO₂ NPs are less efficient under near UV irradiation (4% of the solar spectrum) for effective photocatalysis and recombination of electron-hole pairs than doped TiO₂ NPs. Hence, its use as a photocatalysts for water splitting is limited due to its redox potential referring to the normal hydrogen electrode (NHE),⁵ A lot of studies have been made to increase the photocatalytic activity of titanium dioxide for the water splitting reaction. For this purpose, scientists are working on the synthesis of doped

^aGlobal Academy of Technology, Rajarajeshwarinagar, (off Mysore Road), Ideal Homes Township, Bangalore-560098, Karnataka, India. E-mail: jaiguruj8789@gmail.com; ravishankar8789@gmail.com

^bLaboratory of Thin Films and Nanostructure Fabrication (L3F nano), Institute of Physics, Universidade Federal do Rio Grande do Sul, UFRGS, Avenida Bento Gonçalves 9500, P. O. Box 15051, 91501-970 Porto Alegre, RS, Brazil

^cDayananda Sagar Academy of Technology and Management, Udayapura, Opp Art of Living, Kanakapura Road, Bangalore-560082, India

^dDepartment of Sustainable Chemistry, School of Chemistry, University of Nottingham, Nottingham, UK

TiO₂ NPs using various methods such as hydrothermal, ionic liquid assisted hydrothermal, sol-gel, co-precipitation, combustion and other strategies.^{6,7} Amongst these methods, the ionic liquid assisted hydrothermal method is considered the most prominent, as room temperature ionic liquids (RTILs) have received extensive attention from both academic and industrial researchers over the past two decades. RTILs possess unique properties such as negligible vapor pressure, a wide liquid temperature range, high thermal stability, and dissolubility in both organic and inorganic compounds, high ionic conductivity and a wide electrochemical window. An important aspect of the interaction of RTILs with nanoparticle precursors involves the nucleation and growth of the NPs.⁸ Metal dopants like Au, Ag, Al, Ce, Nd, Eu, Mo, and Fe as well as non-metal dopants like O, N, and S, have been used to enhance the photocatalytic activity of TiO₂ NPs. Au is one of the most promising dopants which modifies the surface and crystalline structure of TiO₂ and acts as electrons sink and minimizes the recombination of electron-hole pairs and making more carriers available for oxidation or reduction processes on the surface. Due to these properties, Au doped TiO₂ NPs show an enhanced photocatalytic H₂ generation *via* the water splitting reaction, electrochemical detection and photochemical detoxification of hexavalent chromium (Cr⁶⁺) compared to bare TiO₂ NPs.

As Cr⁶⁺ proved to be toxic, carcinogenic and mutagenic, the WHO has set 0.96 mM as the threshold limit in drinking water. So, it is very important to monitor its flux followed by detoxification in various environmental matrices.⁹ So many photochemical and electrochemical methods using Au/TiO₂ particles are reported for detoxification and determination of Cr⁶⁺. But there are no reports utilizing a single material for all three applications such as photocatalytic hydrogen production from water and photochemical as well as electrochemical reduction of Cr⁶⁺ to Cr³⁺.

In this manuscript, we report the ionothermal synthesis of Au/TiO₂ NPs and explore the possibility of utilizing the synthesized materials for photocatalytic hydrogen production from water, photochemical detoxification of Cr⁶⁺ to Cr³⁺ as well as for the electrocatalytic reduction of Cr⁶⁺ to Cr³⁺. The catalytic electrochemical reduction is utilized in an amperometric detection of Cr⁶⁺ in various environmental effluents.

Experiment and methods

Chemicals and reagents

Titanium(IV) isopropoxide and tetrachloroaurate(III) trihydrate were purchased from Sigma Aldrich, sodium hydroxide (NaOH) was purchased from Merck, India. 1-(2-Methoxyethyl)-3-methylimidazolium methane sulfonate ionic liquid was prepared by previously developed method.¹⁰ Double distilled water was used throughout the experiments.

Preparation of photocatalysts

For the syntheses of pristine TiO₂ NPs (NPs), 5.5 mL of titanium(IV) isopropoxide, used as precursors. In first step, precursor was added separately in Teflon tube having 2.5 mL 1-

(2-methoxyethyl)-3-methylimidazolium methane sulfonate as IL and 3.5 mL of 0.1 M NaOH solution as mineralizer. The system was left for homogenization under a constant stirring and after that; 8 mL of water was added for the hydrolysis to occur. Furthermore, the precipitate in Teflon tube was put into the stainless autoclave followed by hydrothermal treatment at 130 °C for one day. After the reaction, the system was cooled to room temperature naturally. In the second step, the obtained product was mixed with acetonitrile and stirred for overnight to remove the IL's residue. Finally, TiO₂ NPs were retrieved from centrifugation; thereby, post calcinations step was followed at 300 °C for 1 h for both of the catalysts.

The Au incorporated TiO₂ NPs were prepared by following the similar procedures and post calcinations except for the first step once we mixed different concentrations (0.25, 0.5 and 0.75 wt%) of tetrachloroaurate(III) trihydrate with a fixed volume of titanium tetrachloride (5.5 mL).

Photocatalytic H₂ production

Photocatalytic activities were evaluated by measuring hydrogen production using gas chromatography at room temperature in water ethanol system. Photocatalytic H₂ production reactions were carried out in a closed gas-circulating system as depicted in Fig. 1.¹¹ The reaction was carried out in a closed gas circulating system in an inner irradiation type reactor. Different photocatalysts (10 mg) were sonicated for 20 min to disperse in 7.5 mL aqueous solution. After sonication, 2.5 mL ethanol was added as a sacrificial reagent. Prior to irradiation, the system was deaerated by bubbling argon for 10–15 min to reduce the oxygen content. During the entire experiment, the reaction temperature was kept at 25 °C by eliminating the contribution of IR radiation with the circulation of water in the outer jacket of the reactor. 240 W Hg-Xe arc lamp (Cermax) was used as the UV excitation source, A 300 W Xe arc lamp, with the incident photon flux I_0 of 0.056176 or 0.078245 $\mu\text{mol cm}^{-2} \text{s}^{-1}$, was focused through a shutter window and a 420 or 390 nm cut-off filter onto the window face of the cell was used as the visible light source. Analyses were conducted using Agilent 6820 GC Chromatograph equipped with a thermal conductivity detector (TCD) and a 5 Å molecular sieve packed column with argon as the carrier gas. Using a gastight syringe with a maximum volume of 50 μL , the amount of hydrogen produced was measured for 0.5 h intervals.

Electrochemical monitoring of Cr⁶⁺ in aqueous samples

Nafion coated Au doped TiO₂ modified glassy carbon electrode. Prior to modification, glassy carbon electrode (3 mm diameter) was polished on micro cloth with 1.0, 0.3 and 0.05 micron size alumina. Then the electrode was sonicated in water for about 10 min followed by ethanol. Finally, the electrode was allowed to dry at room temperature. About 10 mg of Au/TiO₂ NPs composite was dispersed well in the solution (2 mL distilled water + 10 mL 0.2% Nafion) by sonication for 30 min. Then 20 mL of the above suspension was cast onto the pre-treated glassy carbon electrode and allowed to dry for 2 h at room temperature.



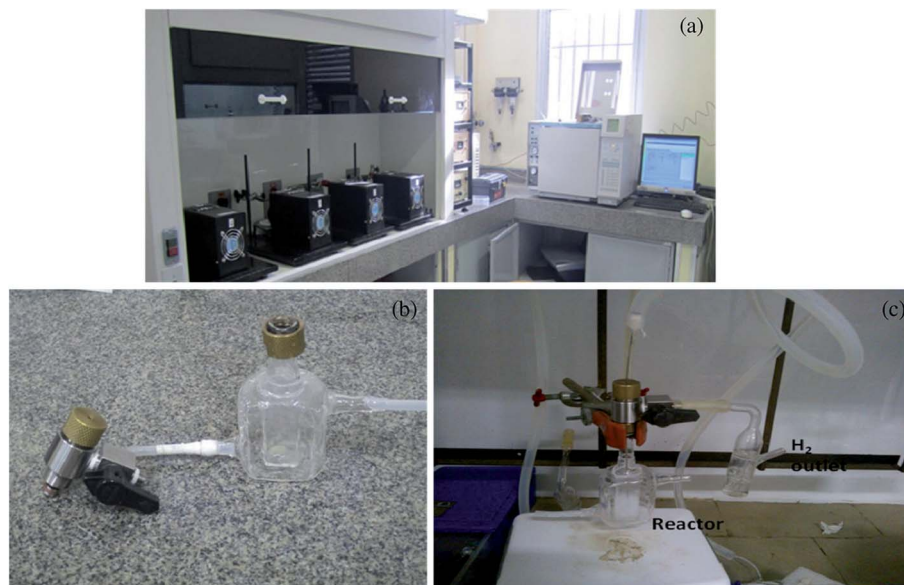


Fig. 1 Experimental set-up picture of photocatalytic hydrogen generation.

Amperometric measurements were performed in a stirred solution with an applied potential of 0.29 V. The electrolyte was deaerated with nitrogen gas for 30 min before each measurement. Aliquot of tap water was directly injected into the electrolyte (0.1 M HCl) for amperometric analysis of Cr^{6+} whereas the lake water samples were filtered using Whatman filter paper before analysis.

Photocatalytic reduction of Cr^{6+} to Cr^{3+} . Photocatalytic experiments were carried out in a 150×75 mm batch reactor with an intensity of sunlight $\sim 950 \text{ W m}^{-2}$ and UV light with 125 W m^{-2} intensity. An aqueous suspension was prepared by adding 0.1 g Au/TiO_2 NPs to 100 mL (1 mM) $\text{K}_2\text{Cr}_2\text{O}_7$ solution with pH 4, the initial pH was adjusted by the addition of 0.05 M H_2SO_4 . During the photocatalytic experiments, the slurry composed of the solution and catalyst was placed on the reactor and stirred magnetically for agitation with simultaneous exposure to both Sun and UV-light for 60 min. A known volume (3 mL) of the exposed solution was withdrawn at specific intervals of time (30 min). Au/TiO_2 NPs were removed from the solution by centrifugation to assess the extent of reduction. The concentration of the $\text{K}_2\text{Cr}_2\text{O}_7$ solution was measured using a UV-visible spectrophotometer.

Characterization

Powder X-ray diffraction data was recorded on Philips X'pert PRO X-ray diffractometer with graphite monochromatized Cu-K_α (1.5418 \AA) radiation operated at 40 kV and 30 mA. X-ray photo electron spectroscopy (XPS) analysis was carried out on an ESCALAB 250 (Thermo-VG Scientific), using Al K_α as the excitation source. The binding energy (BE) from the advantageous carbon (284.6 eV) was used to calibrate the spectra. The absorption spectra of the samples were measured by dispersing the NPs in water using Perkin Elmer Lambda-750 UV-Vis spectrometer. The morphology was examined using table top

Hitachi 3000 scanning electron microscopy (SEM). The nano-structure of the product was observed by transmission electron microscopy (TEM) performed by JEOL JEM 1200 Ex operating at 100 kV. Samples for TEM were prepared by dropping the dispersion of 2-propanol metal oxide nanoparticle on a holey carbon grid and drying the grids under vacuum for 24 h. BET surface area *i.e.* N_2 adsorption-desorption measurements of the samples were measured using Tristar II, Micromeritics. Electrochemical measurements were performed on a standard three-electrode electrochemical cell with a CHI 800 electrochemical workstation (CH Instrument, USA) with a Au/TiO_2 NPs modified glassy carbon electrode as the working electrode, a platinum wire as the counter electrode and a saturated calomel electrode (SCE) as the reference electrode, respectively. All pH measurements were carried out using a digital pH meter MK VI of Systronics make.

Results and discussion

XRD studies

XRD is mainly used to investigate the phase composition and crystallite size of prepared materials. The powder XRD patterns of the Au/TiO_2 NPs prepared by homogenous hydrolysis of titanium(IV) isopropoxide are shown in Fig. 2. All of the patterns are indexed as a single phase of anatase and diffractograms are in good agreement with JCPDS no. 2-387, which clearly confirms the formation of TiO_2 , no diffraction peaks of other polymorphs of titania are observed. All of the NPs give similar patterns without any peak due to the doping of Au. Hence at these loadings, Au particles become uniformly dispersed and therefore do not have adequate dimensions to produce their characteristic patterns. The presence of Au content in TiO_2 nanocrystalline structure influences the particle size, surface area, band gap energy and quantum yield of prepared photocatalysts.



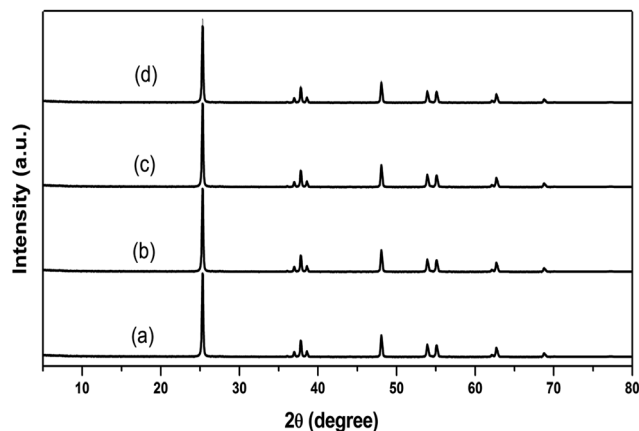


Fig. 2 XRD patterns of (a) pristine TiO_2 NPs, (b) 0.25, (c) 0.5 and (d) 0.75 wt% Au/TiO_2 NPs. The samples were calcinated at 400°C for 1 h.

Crystallite size, BET surface area, band gap energy and quantum yield

The crystallite size, BET surface area, band gap energy and quantum yield for the pristine TiO_2 NPs, 0.25, 0.5, and 0.75 wt% Au incorporated TiO_2 NPs (Au/TiO_2 NPs) were calculated and are shown in Table 1. It can be seen that the Au/TiO_2 NPs present a higher surface area compared to the pristine TiO_2 NPs. In addition, the 0.5 wt% Au/TiO_2 NPs presents the highest surface area compared to all the other photocatalysts. Furthermore, comparing the quantum yields of the Au/TiO_2 NPs and pristine nanomaterials, the Au/TiO_2 NPs seem to be more attractive for photolysis compared to pristine NPs (Table 1). The optical properties were characterized at room temperature using a UV-Vis spectrophotometer in the wavelength range of 200–800 nm and the band gap energies of the NPs were calculated from diffused reflectance spectra using the Tauc plot function, and the results are indicated in Table 1.

XPS studies

The surface chemical composition and the oxidation state for 0.5 wt% Au/TiO_2 NPs sample is investigated by XPS measurements as shown in Fig. 3. From the survey spectrum (Fig. 3(d)) the presence of Ti, O and Au elements was recorded. From the Fig. 3(a) it is made clear that XPS measured at the Ti 2p core levels, the binding energies of 458.6 and 464.1 eV are indicative of Ti 2p_{3/2} and Ti 2p_{1/2} which correspond to Ti^{4+} .⁷ In O 1s region (Fig. 3(b)) the peak centered at 529.6 eV is related to the oxygen

in TiO_2 lattice. However, the adjacent peak at 531.4 eV can be regarded as the presence of surface hydroxide species that were found to be advantageous for improved hydrogen generation.¹² In Au 4f region (Fig. 3(c)), the binding energies for Au 4f_{7/2} and Au 4f_{5/2} are observed at *ca.* 84.1 and 87.5 eV, respectively this indicates that the presence of metallic state Au in TiO_2 lattice structure.¹³

Photocatalytic water splitting hydrogen evolution

The pristine TiO_2 NPs and Au/TiO_2 NPs were subsequently applied for hydrogen evolution in water–ethanol system. Fig. 4 compares the gas chromatography results of the photocatalysts. It can be seen that the pristine NPs prepared in the current study have shown enhanced photoactivity compared to the commercially available powders that highlights the importance of the RTILs synthesis route. Furthermore, the photocatalytic activity of Au/TiO_2 NPs is better than the pristine TiO_2 NPs this presenting Au/TiO_2 NPs as promising photocatalysts. For the Au/TiO_2 NPs, the concentration of Au in TiO_2 matrix has an obvious effect on the H_2 evolution activity that has an optimum for 0.5 wt% concentration of Au evolving $3344 \mu\text{mol g}^{-1}$ of H_2 . On the other hand, the H_2 evolution rate dropped to $2054 \mu\text{mol g}^{-1}$ for 0.75 wt% Au/TiO_2 NPs.

Photocatalytic hydrogen generation by 0.5 wt% Au/TiO_2 NPs in UV light and visible light is presented in Fig. 5. It can be observed that 0.5 wt% Au/TiO_2 NPs show 2136 and $3344 \mu\text{mol g}^{-1}$ of hydrogen generation when exposed to UV illumination and visible light illumination, respectively. The enhanced photocatalytic hydrogen generation of 0.5 wt% Au/TiO_2 NPs in visible light illumination may be attributed to its band gap, quantum efficiency, surface area and surface morphology. The enhanced photocatalytic activity of Au/TiO_2 NPs can be explained as follow; water splitting is an uphill reaction that needs the standard Gibbs free energy change of ΔG° of 237 kJ mol^{-1} or 1.23 eV .^{14,15} Therefore, the band gap energy (E_g) of the photocatalyst should straddle the water redox potentials and it should be between $1.23 \text{ eV} < E_g < 3.26 \text{ eV}$.^{16,17} In addition, the photocatalyst should be efficient enough to separate the photogenerated carriers and to transport them to their reactive sites in order to decrease the electron–hole pair recombination. In Au/TiO_2 NPs that possess appropriate band gap energetic the CB electrons of one semiconductor are injected to other thereby; achieving a wide electron–hole separation (Fig. 6).^{18,19} The CB of TiO_2 and Au are positioned at *ca.* -0.7 and -0.30 V , respectively more negative than that of water reduction potential and VB of TiO_2 lies closed to the water oxidation potential

Table 1 Crystalline size, BET surface area, quantum yield and band gap energies of the different photocatalysts synthesized via ionic liquid assisted hydrothermal method

Samples	Au content (wt%)	Crystalline size (nm)	BET surface area ($\text{m}^2 \text{g}^{-1}$)	Quantum yield	Band gap (eV)
TiO_2 NPs	0	30.3 for (101)	34.1	0.22	3.31
Au/TiO_2 NPs	0.25	35.3 for (101)	38.6	0.38	2.7
	0.5	36.7 for (101)	52.7	0.51	2.10
	0.75	35.1 for (101)	41.8	0.40	1.98



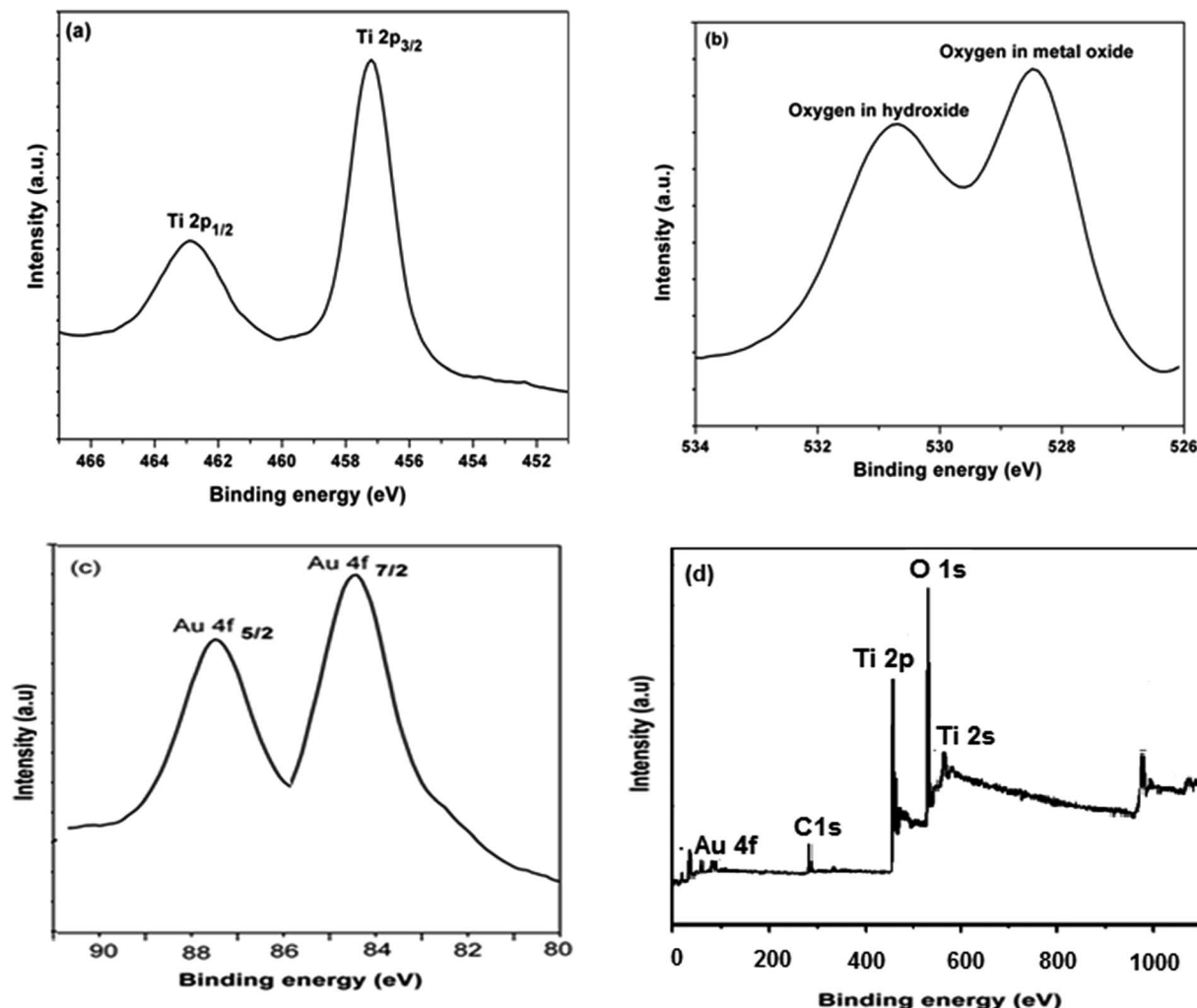


Fig. 3 XPS spectra of (a) Ti 2p (b) O 1s, (c) Au 4f and (d) survey spectrum of 0.5 wt% Au/TiO₂ NPs.

compared to the VB of Au.^{20–22} Therefore, owing the advantage of Au/TiO₂ NPs, under illumination; electrons are excited from VB to CB of TiO₂, thereof transferred to the CB of Au, thereby;

reducing water to hydrogen. On the other hand holes from the VB of TiO₂ oxidize water. Therefore, the hetero-junction formed between TiO₂ and Au efficiently separates the photoexcited electron-hole pairs, and thus hinders the charge recombination and improve the photocatalytic performance of Au/TiO₂ NPs compared to the pristine TiO₂ NPs. Since we are changing the concentration of Au that evidently affects the capture of photoexcited electrons from the CB of TiO₂. If concentration of Au is large, the light absorption from TiO₂; will be small thereby inhibiting the generation of electron-hole pairs in TiO₂ that is the main reason of decreasing H₂ evolution rate of high content incorporation of Au such as that 0.75 wt% of Au in TiO₂ matrix. In the absence of Au, most of these charges tend to recombine rapidly as the pristine TiO₂ NPs present lower photocatalytic hydrogen generation. Therefore, the synergy for improved photocatalytic activity can be obtained only for a certain concentration of Au in TiO₂ matrix. In the current work that synergy is achieved for the 0.5 wt% Au/TiO₂ NPs. Therefore, the optimum concentration of Au in TiO₂ matrix not only optimize the light absorption but also increase the BET surface area and quantum yield (Table 1) which than synergize 0.5 wt% Au/TiO₂

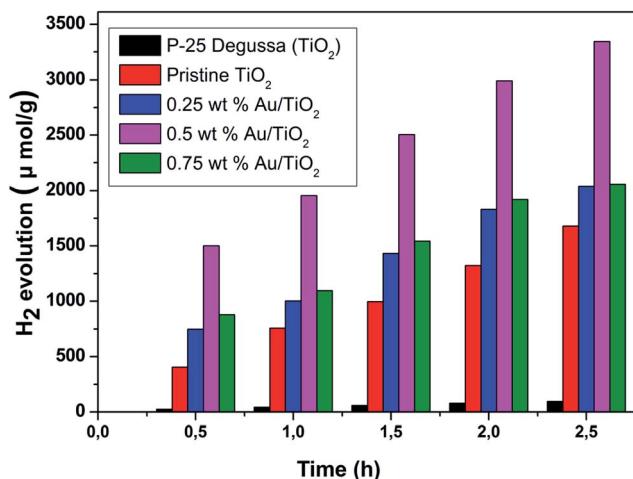


Fig. 4 Hydrogen generation of pristine TiO₂ NPs, 0.25, 0.5, 0.75 wt% Au/TiO₂ NPs and commercial TiO₂ (Degussa P-25).



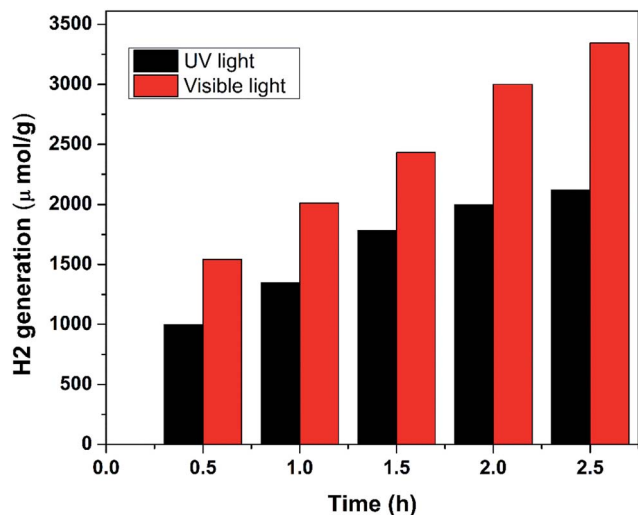


Fig. 5 Comparison study of photocatalytic hydrogen generation of 0.5 wt% Au/TiO₂ NPs under illumination of UV and visible light.

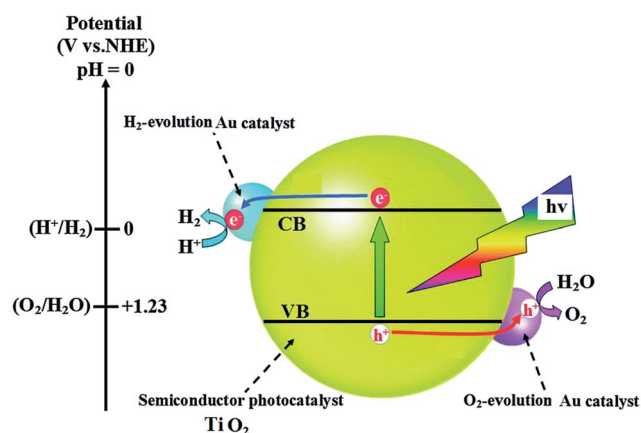


Fig. 6 Electron transportation in Au/TiO₂ NPs for photocatalytic hydrogen generation.

NPs for enhanced photocatalytic activity compared to all other samples.

As it provided the best results in all aspects of the current study, we then characterized the 0.5 wt% Au/TiO₂ NPs comprehensively.

The gold content in the synthesized Au/TiO₂ samples, measured by ICP-OES analysis is presented in Table 2. The

Table 2 Gold content in Au/TiO₂ samples

Sl. no	Sample	Au (mol%)	
		Input ^a	Output ^b
1	0.25 wt% Au/TiO ₂	0.25	0.23
2	0.50 wt% Au/TiO ₂	0.50	0.48
3	0.75 wt% Au/TiO ₂	0.75	0.73

^a [mol of Au × 100]/mol of Ti in solution during hydrolysis. ^b Calculated from Au wt%, obtained from ICP analysis.

estimated gold contents in the samples were found to be in good agreement with the theoretical values.

Surface morphology studies

The surface morphology of 0.5 wt% Au/TiO₂ NPs as showed in Fig. 7(a), 0.5 wt% Au/TiO₂ NPs was analyzed using SEM and it shows irregularly-shaped particles, which aggregated to form crystals. The quantitative compositional analysis of 0.5 wt% Au/TiO₂ NPs is analyzed using energy dispersive X-ray (EDAX) spectroscopy measurements. The spectra confirm the presence of basic elements like Ti, O and Au, as shown in Fig. 7(b). From the measurements, it is enumerated that the Au was successfully inserted in to the TiO₂ crystalline structure. The transmission electron microscopic analysis was carried out to confirm the size of the particles, growth pattern and distribution of the crystallites. A representative TEM image in Fig. 7(c) shows that most of the particles are well distributed with little concentration of aggregates, the average particle size was found to be 38 nm. The lattice spaces of 0.35 nm and 0.239 nm can be observed in HRTEM image (Fig. 7(d)), that are in good agreement with (101) for anatase TiO₂, (111) plane for Au. The corresponding SAED spectrum is shown in Fig. 7(e) that further indicates the presence of Au in TiO₂ crystalline structure.

Photocatalytic reduction of Cr⁶⁺ to Cr³⁺

Effect of initial concentration. The effect of initial Cr⁶⁺ concentrations on its photo reduction rate was investigated over the range of 5 to 25 ppm at the optimal conditions of pH 2 and 1.0 g/0.1 L of Au/TiO₂ (Fig. 8(a)). It is clearly noted that the irradiation time required for complete removal of Cr⁶⁺ under light source was extended as the initial Cr⁶⁺ concentration increased. This can be rationalized according to Beer–Lambert's law, as Cr⁶⁺ concentration increases, the path length of photons entering into the reaction mixture decreases, and a fewer photons reach the catalyst surface. As the incident intensity, catalyst amount and irradiation time are constant, therefore, the availability of active sites will be reduced. Consequently, the photo-reduction rate of Cr⁶⁺ decreases as the concentration increases.²³ Moreover, an increase in Cr⁶⁺ concentrations can lead to the saturation of the limited number of accessible active sites on the photocatalyst surface and/or deactivation of the active sites of the catalyst, resulting in a reduction in the photo reduction rate.

Effect of catalyst dose. In a typical photocatalytic experiment, it is essential to determine the minimum amount of catalyst required to remove the maximum amount of pollutants. Therefore, the influence of Au/TiO₂ dose on photo-reduction of Cr⁶⁺ was investigated in order to attain the maximum absorption of efficient solar light photons as well as to avoid an ineffective excess amount of the photocatalyst. Fig. 8(b) shows the photo-reduction rate of 5 μg L⁻¹ of Cr⁶⁺ at the optimum pH 4 using various amounts of Au/TiO₂ NPs under illumination of light source. The photocatalytic reduction rate of Cr⁶⁺ increased with the increase in catalyst dose from 0.25 to 1.0 g/0.1 L. Further increment in catalyst loading to 1.25 g/0.1 L leads to decrease in photo-reduction efficiency. The observed increment



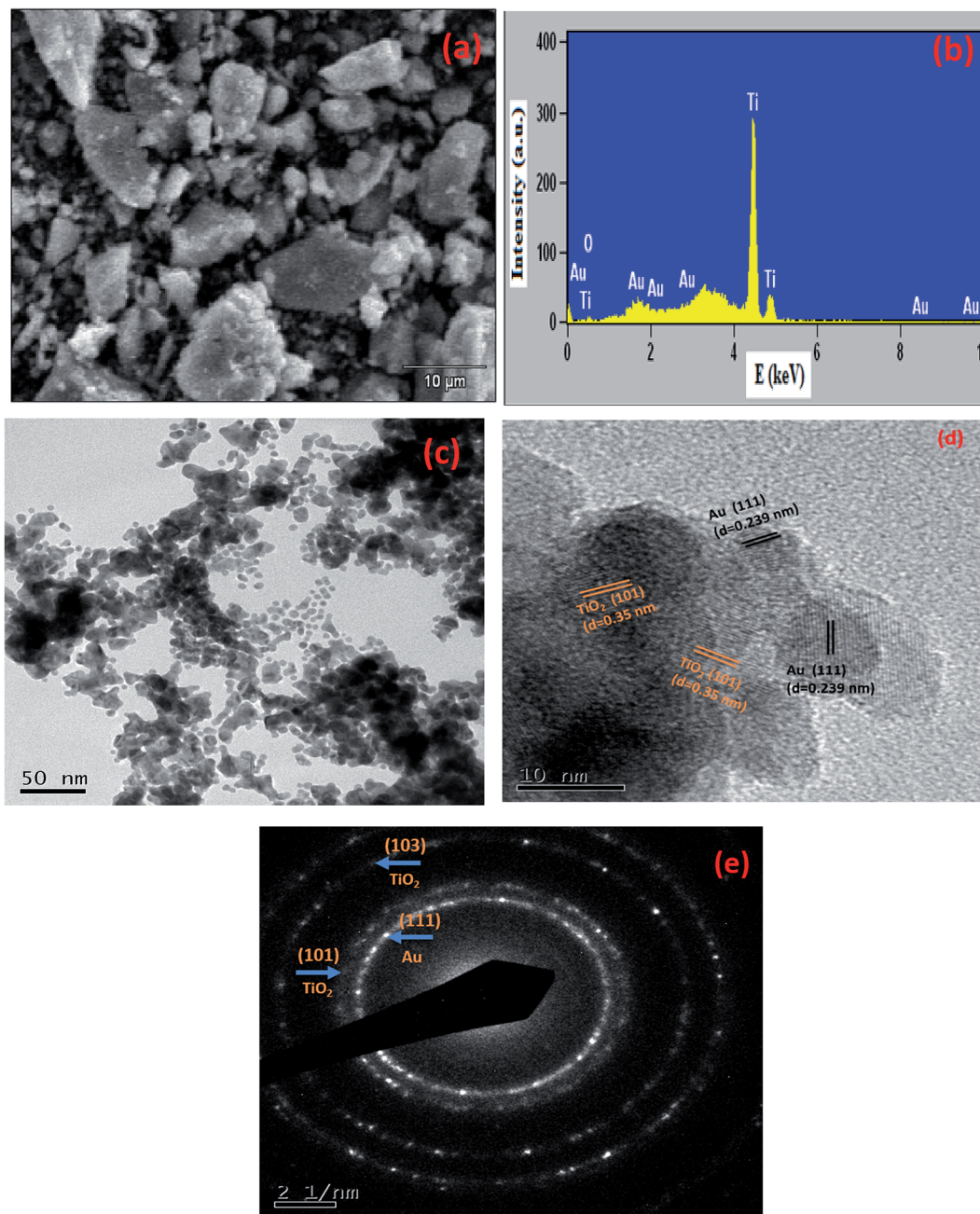


Fig. 7 (a) SEM image, (b) EDAX, (c) TEM image, (d) HRTEM image and (e) SAED pattern of the 0.5 wt% Au/TiO₂ NPs.

in the photo-reduction efficiency at the catalyst concentration of 1 g/0.1 L is due to the increase of the total number of active sites on the photocatalyst surface thus causing an increase in the number of e^- which can take part in the photo-reduction of Cr^{6+} . At catalyst loading beyond the optimum, the tendency toward particles aggregation increases, resulting in a reduction in surface area available for light absorption and hence a drop in photocatalytic degradation rate.²⁴ Furthermore, the increase of the turbidity of the suspension reduces light penetration due to the enhancement of light scattering; the result is the decrease of the number of activated sites on the TiO₂ surface and shrinking of the effective photoactivated volume of suspension. The interaction of

these two processes resulted in a reduced performance of photocatalytic performance with the overloaded catalyst.

Effect of pH. pH of the solution plays a major role in the photocatalytic reaction as it is known to influence the surface charge of the semiconductor thereby affecting the interfacial electron transfer and the photo-redox process.²⁵ The possible functional groups on TiO₂ surface in water are $TiOH_2^+$, $TiOH$, and TiO^- . The point of zero charge (pH_{pzc}) of TiO₂ is an important factor determining the distribution of the surface groups. The surface of TiO₂ is negatively charged with the species TiO^- when pH is higher than pH_{pzc} . On the contrary, it is positively charged with the species $TiOH_2^+$. Fig. 8(c) depicts



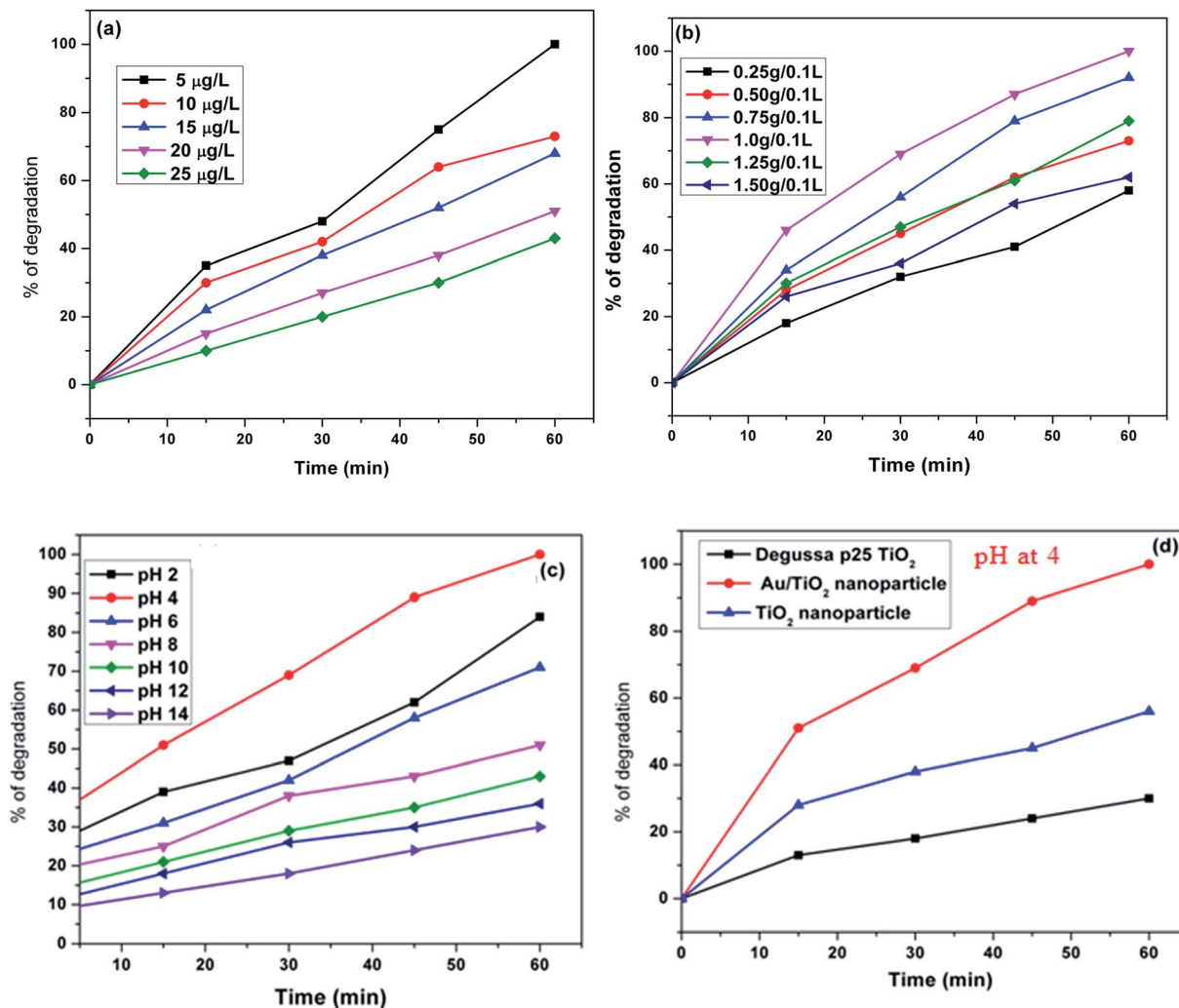


Fig. 8 (a) Effect of dye concentration, (b) effect of catalytic load, (c) effect of pH on the photocatalytic reduction of Cr^{6+} to Cr^{3+} and (d) comparison study of photocatalytic reduction of Cr^{6+} to Cr^{3+} by different photocatalysts.

the effect of pH on the photocatalytic reduction rate of Cr^{6+} . It is worth noting that, the removal rate of Cr^{6+} decreased with increasing the initial pH value from 2 to 14. The higher removal efficiency at pH 4, which is lower than the point of zero charge (pH_{pzc}) of TiO_2 , can be attributed to the strong electrostatic attraction between the anionic chromate species (CrO_4^{4-} and/or HCrO_4^-) and the positively charged TiOH_2^+ surface. On the other hand, at higher pH value the TiO_2 surface is negatively charged in a state of TiO^- and $\text{Cr}_2\text{O}_7^{2-}$ becomes dominate species, which may be repelled away from the TiO_2 surface which subsequently leads to inhibited adsorption of Cr^{6+} . Furthermore, Cr^{3+} will be precipitated on the surface of TiO_2 as $\text{Cr}(\text{OH})_3$ at increased solution pH, covering the activity sites of the catalyst.²⁶ As a result, Cr^{6+} the photo reduction efficiency decreases in alkaline medium.

Comparative study of photocatalytic activity of Degussa p25 TiO_2 , TiO_2 and Au/TiO_2 NPs

Fig. 8(d) shows the comparative study of photocatalytic activity of Degussa p25 TiO_2 , TiO_2 and Au/TiO_2 NPs. Photocatalytic

reaction was carried out at constant Cr^{6+} concentration ($5 \mu\text{g L}^{-1}$), constant catalytic load ($1 \text{ g}/0.1 \text{ L}$) and pH at 4. These studies indicate the photocatalytic activity of Au/TiO_2 NPs were superior to the photocatalytic activity of bare TiO_2 NPs and Degussa p25 TiO_2 this was attributed to its surface morphology, higher surface area and quantum yield than TiO_2 NPs and Degussa p25 TiO_2 .

The effect of Au doping on the photocatalytic activity of TiO_2 NPs

TiO_2 under irradiation of UV light produces electron-hole pairs, recombination of electron-hole pairs more in the case of bare TiO_2 nanoparticles; the rate of photocatalytic activity resulting there is a reduction of H_2 evolution and photo-reduction of Cr^{6+} . The positive effect of Au on the photocatalytic activity of TiO_2 may be explained by its ability to trap electrons.^{27,28} This process reduces the recombination of light generated electron-hole pairs at the TiO_2 surface and availability of electron and hole in the respective conduction and reduction bands increases.²⁹ Therefore a more effective electron transfer occurs to the



electron acceptors and donors adsorbed on the surface the particle than in the case of bare TiO_2 . Oxygen adsorbed on the photocatalyst surface traps the electrons and produces superoxide anion and on the other hand holes at the TiO_2 surface can oxidize adsorbed water or hydroxide ions to radicals. The enhanced photocatalytic activity of Au/TiO_2 NPs can also be explained by the oxidation state of Au ion on the surface of TiO_2 .³⁰ The Au deposited at the surface as Au^+ and Au^{2+} ions, the reduction of Au ions to metallic Au consumes electrons. Therefore the electron-hole pair recombination reduces and it showed that the electron scavenging by the oxygen at the surface the excited semiconductor particle cannot efficiently complete with the electron transfer to the Au ion.³¹ So electron transfer to the Au ion is a rather fast comparing to electron transfer to oxygen molecule, the loaded Au metals on the TiO_2 surface can expedite the transport of photo-generated electrons to the outer systems. And it can be showed the in the Fig. 6. Mechanistic pathway of photocatalytic reduction from Cr^{6+} to Cr^{3+} as shown in Scheme 1.

Photochemical detoxification of Cr^{6+} to Cr^{3+} in the presence of sunlight and UV light

Photochemical detoxification of Cr^{6+} to Cr^{3+} in the presence of sunlight and UV light is shown in Fig. 9, respectively. Our catalyst is found to be more active in sunlight compared to UV light. The photocatalytic reduction of $\text{K}_2\text{Cr}_2\text{O}_7$ (0.1 M) having pH 4 was carried out by adding 0.1 g Au/TiO_2 NPs into a photocatalytic reactor in sunlight; it is clear that within 60 min about 96% reduction was achieved, whereas in UV light about 60% reduction was achieved. This clearly indicates that our material showed good photocatalytic reduction from Cr^{6+} to Cr^{3+} in sunlight compared to the UV-light. This may be due to the decrease in the band gap of TiO_2 particles achieved by doping of Au.

Effect of recycling of the photocatalyst

Effect of recycling of 0.5 wt% Au/TiO_2 nanoparticles on photocatalytic reduction of Cr^{6+} to Cr^{3+} and photocatalytic hydrogen generation and Fig. 10(a) shows the effect of recycling of 0.5 wt% Au/TiO_2 nanoparticles for photocatalytic reduction of Cr^{6+} to Cr^{3+} , prepared at 130 °C for 1 day using an ionic liquid assisted hydrothermal method. One of today's main industrial wastewater treatment strategies is focused on the development of green technologies. Recycling of the Au/TiO_2 nanoparticles

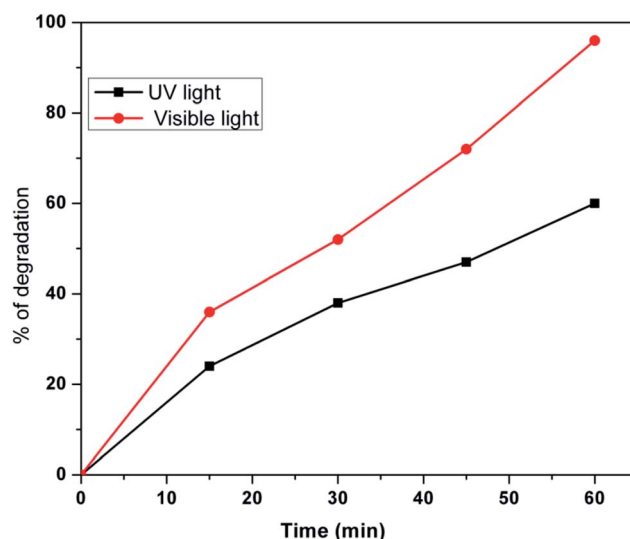


Fig. 9 Photochemical detoxification of Cr^{6+} to Cr^{3+} in the presence of sunlight and UV lights.

can be foreseen as good practice for sustainable industrial waste treatment. Consequently, it is necessary to demonstrate whether after a photocatalytic treatment the catalyst can be reused. The nanoparticles were used and recycled consecutively five times. The photocatalytic reaction was carried out at a constant Cr^{6+} concentration ($10 \mu\text{g L}^{-1}$) and constant catalytic load (1 g/0.1 L of Cr^{6+} solutions). Once the first set of experiments is completed, the catalyst is retrieved from the solution *via* centrifugation and dried in an oven. The recycled catalyst was used for the second cycle and so on. This experimental study indicated that the rate of photocatalytic reduction of Cr^{6+} to Cr^{3+} not decreased so much as the number of cycles increased. The effect of photocatalytic reduction of Cr^{6+} to Cr^{3+} for first cycle is almost same as fifth cycle, slight decrease in the photocatalytic activity could be due to aggregation and sedimentation of the dye around Au/TiO_2 after each cycle of photocatalytic experiment. Each time the catalyst is reused; new parts of the catalyst surface become unavailable for Cr^{6+} adsorption and, thus, photon absorption, reducing the efficiency of the catalytic reaction, the same way results also observed for the effect of recycling of 0.5 wt% Au/TiO_2 nanoparticles for photocatalytic hydrogen generation as shown in the Fig. 10(b).

Form the above analyses it was cleared that the prepared Au/TiO_2 photocatalyst showing good photo stability.

Electrochemical reduction studies of Cr^{6+}

Determination of Cr^{6+} by cyclic voltammetry (CV) method. The electrocatalytic properties of the Au/TiO_2 NPs towards Cr^{6+} reduction was evaluated by the CV studies. It was proved that acidic environment plays a crucial role in electrocatalytic reduction of Cr^{6+} .^{32,33} Fig. 11(a) shows the cyclic voltammograms obtained for Cr^{6+} in 0.1 M HCl medium on bare GC as well as Au/TiO_2 NPs composite modified GC. There is an reduction peak around 0.285 V on Au/TiO_2 NPs composite



Scheme 1 Mechanistic pathway of photocatalytic reduction from Cr^{6+} to Cr^{3+} .



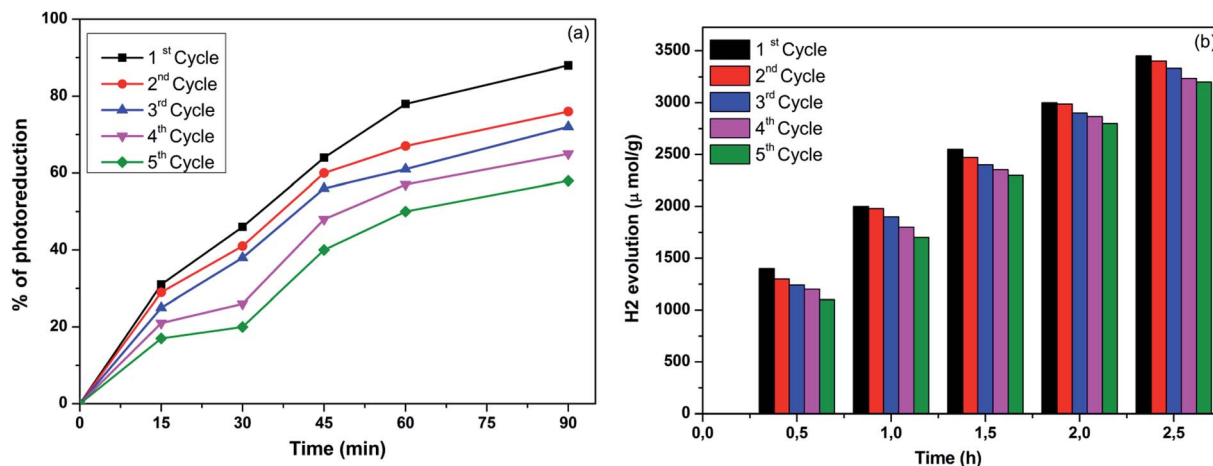


Fig. 10 (a) Effect of recycling test of 0.5 wt% Au/TiO_2 nanoparticles for photocatalytic reduction of Cr^{6+} to Cr^{3+} , (b) effect of recycling test of 0.5 wt% Au/TiO_2 nanoparticles for photocatalytic hydrogen generation.

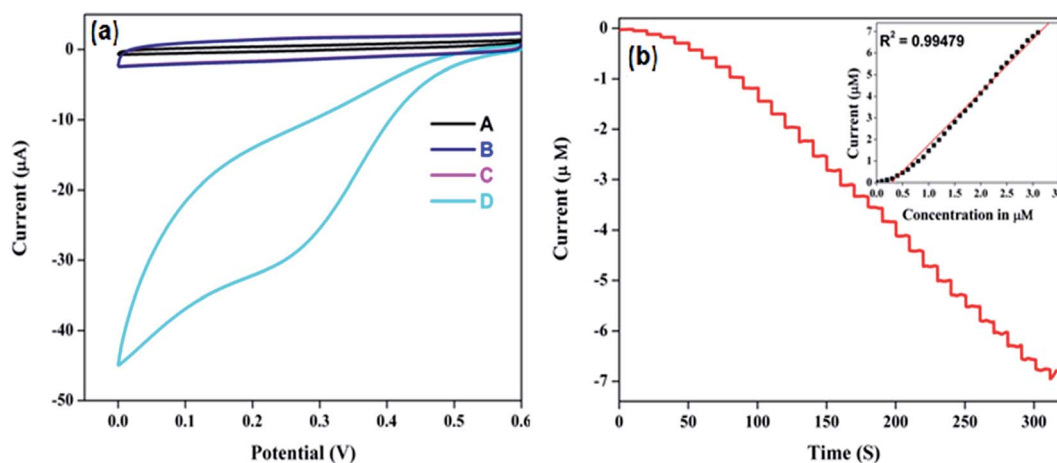


Fig. 11 (a) CV graphs obtained in 0.1 M HCl electrolyte with scan rate 0.1 mV s^{-1} (A) bare glassy carbon electrode (B) 0.5 wt% Au/TiO_2 NPs modified glassy carbon electrode (C) bare glassy carbon electrode +0.1 mM Cr^{6+} and (D) 0.5 wt% Au/TiO_2 NPs modified glassy carbon electrode +0.1 mM Cr^{6+} . (b) Amperometric graphs obtained on the 0.5 wt% Au/TiO_2 NPs modified GC electrode with potential 0.29 V, electrolytic medium 0.1 M HCl and Cr^{6+} (0 to $3.1 \mu\text{M}$).

modified GC where as there is no such peak obtained for same concentration of Cr^{6+} on bare GC electrode. This confirms that the Au/TiO_2 NPs composite materials catalyzed electrochemical

reduction process otherwise the reduction is very insignificant on bare GC and can't be used for detection of Cr^{6+} in microgram levels.

Table 3 Determination of Cr^{6+} in tap water and industrial waste water samples

Sample	Found Cr^{6+} (μM)		Added Cr^{6+} (μM)	Total Cr^{6+} (μM)		Recovery (%)	
	Proposed method	ICP-AES method		Proposed method	ICP-AES method	Proposed method	ICP-AES method
Tap water	Not detected	Not detected	0.5	0.5901 ± 0.090	0.7999	98.56	99.82
	Not detected	Not detected	1.0	0.9776 ± 0.006	0.9486	98.76	99.66
	Not detected	Not detected	2.0	0.9886 ± 0.007	0.9986	98.86	99.87
	Not detected	Not detected	3.0	3.0000 ± 0.201	3.1005	100.02	101.23
Industrial waste water	Not detected	Not detected	0.5	0.4985 ± 0.008	0.5000	99.76	99.99
	Not detected	Not detected	1.0	0.9967 ± 0.001	1.0031	99.86	100.40
	Not detected	Not detected	2.0	0.9896 ± 0.005	0.9996	98.76	99.67
	Not detected	Not detected	3.0	2.7886 ± 0.126	2.7855	99.98	100.00



Determination of Cr⁶⁺ by amperometry. The analytical characteristics of the Au/TiO₂ NPs modified GC electrode towards Cr⁶⁺ monitoring were evaluated by amperometry. Under optimized conditions the method has shown liner range from 0.1 to 3.1 μM with the $R^2 = 0.99879$ (Fig. 11(b)). The response time was very quick and the limit of the detection was found to be 0.01 μM. The obtained detection limit was lesser than that of the WHO value, from this it clear that our protocol can be readily utilized for monitoring the Cr⁶⁺ in drinking water. Then the possible interference from the other reducible species commonly present in natural water samples were studied. To check the practical applicability of the method we had carried out the chromium detection in natural water samples collected from the lakes and in tap waters. The results are presented in Table 3. The chromium was not detected in the tap water as well as lake water samples, then we spiked the samples with Cr⁶⁺ and recovery studies have been carried out and the recovery values are found to be more than 98%. The results obtained with our method were validated by analyzing the samples by ICP-AES technique and the results of proposed method were found to be in good agreement with ICP-AES analysis results.

Conclusions

Au/TiO₂ NPs have been successfully prepared at 130 °C in one day using an ionic liquid assisted hydrothermal method using methoxyethyl methyl imidazolium methanesulfonate as the ionic liquid, titanium(IV) isopropoxide and tetrachloroaurate(III) trihydrate as precursors. Physico-chemical properties of the obtained photocatalysts were investigated *via* thorough characterizations. The framework substitution of Au in TiO₂ NPs was established by XRD, XPS and EDS techniques. XRD and TEM image results confirmed the anatase phase and nano-crystalline nature of Au/TiO₂. The optical properties revealed an extended tailing of the absorption edge toward the visible region upon Au doping. The concentration of Au in TiO₂ matrix has been fine-tuned to improve the hydrogen production, electrochemical detection and photochemical detoxification of hexavalent chromium (Cr⁶⁺). One of the important feature of this article is still there are no reports utilizing a single material for all three applications such as photocatalytic hydrogen production from water and photochemical as well as electrochemical reduction of Cr⁶⁺ to Cr³⁺. The synergy between the Au and TiO₂ has an optimum for concentration of 0.5 wt% Au doped TiO₂. The optimized product has produced promising hydrogen evolution of 3344 μmol g⁻¹ under the illumination of visible light source in water/ethanol system. The optimized product has showed promising electrocatalytic reduction and photocatalytic detoxification ability of the material towards Cr⁶⁺ were explored. Amperometric studies showed a linear range from 0.1 to 2.7 mM, and limits of detection and quantification of 0.01 mM and 0.023 mM, respectively. The Au/TiO₂ nanoparticle modified glassy carbon has been used for electrochemical monitoring of Cr⁶⁺ in natural water samples. The material also showed better photochemical reduction of Cr⁶⁺ in sunlight compared to UV light.

Conflicts of interest

There are no conflicts to declare.

Acknowledgements

One of the authors, Dr T. N. Ravishankar wishes to acknowledge Dr Sherdil Khan for his valuable suggestions, CNPq-TWAS, Brazil, for financial support and Laboratory of Thin Films and Nanostructure Fabrication (L3F nano), Institute of Physics, UFRGS, Brazil for research facilities. Global Academy of Technology, Bangalore, Karnataka, India for encouragement and support.

References

- 1 J. Yu, L. Qi and M. Jaroniec, *J. Phys. Chem. C*, 2010, **114**, 13118–13125.
- 2 Q. Xiang, D. Lang, T. Shen and F. Liu, *Appl. Catal., B*, 2015, **162**, 196–203.
- 3 M. Zhu, P. Chen and M. Liu, *ACS Nano*, 2011, **5**, 4529–4536.
- 4 G. Nagaraju, T. N. Ravishankar, K. Manjunatha, S. Sarkar, H. Nagabhushana, R. Goncalves and J. Dupont, *Mater. Lett.*, 2013, **15**, 27–30.
- 5 C. Liao, C. Huang, C. Jeffrey and S. Wu, *Catalysts*, 2012, **2**, 490–516.
- 6 T. N. Ravishankar, T. Ramakrishnappa, H. Nagabhushana, V. S. Souza, J. Dupont and G. Nagaraju, *New J. Chem.*, 2014, **39**, 1421–1429.
- 7 T. N. Ravishankar, M. O. Vaz, S. Khan, T. Ramakrishnappa, S. R. Teixeira, G. R. Balakrishna, G. Nagaraju and J. Dupont, *New J. Chem.*, 2016, **40**, 3578–3587.
- 8 D. Jose, C. M. Sorensen, S. S. Rayalu, K. M. Shrestha and K. J. Klabunde, *Int. J. Photoenergy*, 2013, 685614.
- 9 T. N. Ravishankar, S. Muralikrishna, K. Sureshkumar, G. Nagaraju and T. Ramakrishnappa, *Anal. Methods*, 2015, **7**, 3493–3499.
- 10 J. Dupont, C. S. Consorti, P. A. Z. Suarez and R. F. de Souza, *Org. Synth.*, 2002, **79**, 236–241.
- 11 A. K. Ramasami, T. N. Ravishankar, G. Nagaraju, T. Ramakrishnappa, S. R. Teixeira and R. G. Balakrishna, *Bull. Mater. Sci.*, 2017, **40**, 345–354.
- 12 T. N. Ravishankar, M. d. O. Vaz, S. Khan, T. Ramakrishnappa, S. R. Teixeira, G. R. Balakrishna, G. Nagaraju and J. Dupont, *ChemistrySelect*, 2016, **1**, 2199–2206.
- 13 S. Shuang, R. Lv, Z. Xie and Z. Zhang, *Sci. Rep.*, 2016, **6**, 26670.
- 14 A. Athanasiou, A. Mitsionis, T. Vaimakis, P. Pomonis, D. Petrakis, L. Loukatzikou, N. Todorova, C. Trapalis and S. Ladas, *Appl. Surf. Sci.*, 2014, **319**, 143–150.
- 15 N. Zhang, Y. Zhang and Y. Xu, *Nanoscale*, 2012, **4**, 5792–5813.
- 16 Q. Xiang, F. Cheng and D. Lang, *ChemSusChem*, 2016, **9**, 996–1002.
- 17 X. Yu, J. Yu, B. Cheng and B. Huan, *Chem.–Eur. J.*, 2009, **15**, 6731–6739.



- 18 D. Lang, T. Shen and Q. Xiang, *ChemCatChem*, 2015, **7**, 943–951.
- 19 Y. Shiraishi, N. Saito and T. Hirai, *J. Am. Chem. Soc.*, 2005, **127**, 12820–12822.
- 20 Q. Xiang, B. Cheng and J. Yu, *Angew. Chem., Int. Ed.*, 2015, **54**, 11350–11366.
- 21 M. M. Khan, S. A. Ansari, D. Pradhan, M. O. Ansari, D. H. Han, J. Lee and M. H. Cho, *J. Mater. Chem. A*, 2014, **2**, 637–644.
- 22 S. A. Ansari, M. M. Khan, M. O. Ansari and M. H. Cho, *New J. Chem.*, 2015, **39**, 4708–4715.
- 23 Y. A. Shaban, *World J. Nano Sci. Eng.*, 2013, **3**, 154–160.
- 24 R. Wang, D. Ren, S. Xia, Y. Zhang and J. Zhao, *J. Hazard. Mater.*, 2009, **169**, 926–932.
- 25 M. C. Lu, G. D. Roam, J. N. Chen and C. P. Huang, *J. Photochem. Photobiol., A*, 1993, **76**, 103–109.
- 26 H. Chen, Y. Shao, Z. Xu, H. Wan, Y. Wan, S. Zheng and D. Zhu, *Appl. Catal., B*, 2011, **105**, 255–262.
- 27 U. M. Jasim, C. Federico, S. Domenica, B. Silvia and Z. Adriano, *Mater. Res. Soc. Symp. Proc.*, 2008, **1077**, 41–47.
- 28 B. Naik, S. Kim, C. Jung, S. Moon, S. H. Kim and J. Y. Park, *Adv. Mater. Interfaces*, 2014, **1**, 1300018.
- 29 D. Jose, C. M. Sorensen, S. S. Rayalu, K. M. Shrestha and K. J. Klabunde, *Int. J. Photoenergy*, 2013, **2013**, 685614.
- 30 W. Zhao, Z. Ai, J. Dai and M. Zhang, *PLoS One*, 2014, **9**, e103671.
- 31 T. Jafari, E. Moharrerri, A. S. Amin, R. Miao, W. Song and S. L. Suib, *Molecules*, 2016, **21**, 900.
- 32 P. M. Hallam, D. K. Kampouris, R. O. Kadaraand and C. E. Banks, *Analyst*, 2010, **135**, 1947–1952.
- 33 J. P. Metters, R. O. Kadara and C. E. Banks, *Analyst*, 2012, **137**, 896–902.

